Acta Scientiarum
http://periodicos.uem.br/ojs
ISSN on-line: 1807-8664
Doi: 10.4025/actascitechnol.v46i1.65406

Mechanical analysis and materials selection of a scissor lift system for pig transportation

Lívia Valentim Sanches, Celso Antonio Goulart, Priscilla Ayleen Bustos MacLean and Lucia Adriana Villas-Bôas*

[1]Departamento de Engenharia de Biossistemas, Faculdade de Ciências e Engenharia, Universidade Estadual Paulista, Rua Domingos da Costa Lopes, 780, 17602-496, Tupã, São Paulo, Brazil. *Author for correspondence. E-mail: lucia.villas-boas@unesp.br

ABSTRACT. Pigs can experience stressful moments during handling practices before arrival at the slaughter location, so adequate handling plays a crucial role in pig response to preslaughter stress. This work presents preliminary mechanical analysis and materials selection of a scissor lift system with the purpose of loading and unloading pigs for transport. The scissor lift offers a simple design and is frequently used as a lifting mechanism in the automotive, aerospace, advanced manufacturing, and transportation industries due to its flexibility to adapt to different uses. The design and mechanical analysis of the proposed scissor lift mechanism were performed to carry pigs ranging from 80 to 180 kg with a working height from 1 to 1.2 m to meet the first-floor height of traditional trucks. The model and the components of the system were dimensioned to ensure the well-being of the animals, avoid injuries, and reduce the stress that negatively affects meat quality. The structural analysis of the system was developed through classical analytical calculations in association with materials selection. The proposed design is apt to load and unload pigs safely and be used with different types of trucks.

Keywords: scissor lift; static analysis; materials selection; pig transportation; animal welfare.

Received on October 13, 2022.
Accepted on January 25, 2023.

Introduction

Brazilian swine production plays a vital role in food production and stands out in the national economy as being consolidated and rapidly expanding livestock activity. According to the *Ministério da Agricultura e Pecuária* (Mapa, 2021), Brazil ranks fourth in pig production and exportation worldwide, and gathers all conditions to move further up in this rank. Projections from Mapa show that pork has the potential to reach an annual production growth rate of 3% in the period from 2020/21 to 2030/31, and become the second most consumed animal protein nationally, with a projected annual consumption growth rate of 2.1% in the coming years (Mapa, 2021). International demands are also expected to strongly contribute to the growth in production and consumption in the next ten years (Barcellos et al., 2011; Zanella, 2017; Mapa, 2021).

Brazilian pig farming contributes positively to the national economic development and is competitive on national and international scales, especially in slaughtering and processes of meat processing agroindustry. However, the country still faces obstacles due to expensive costs and inefficient logistics related to some steps in these activities (Costa et al., 2016; Zanella, 2017). Besides, good production practices regarding animal welfare must be widely adopted so that the national pig industry maintains its competitiveness in the global scenario since the quality of final products is directly connected to the pigs' health and is essential in the search for a balance between increased profit margins and sustainability (Costa et al., 2016; Ludtke, Costa, Rohr, & Costa, 2016; Zanella, 2017).

Transportation is an important, essential, and inevitable process in the multi-stage pig industry and is considered one of the most stressful events for pigs before slaughter. Excessive stress may result in economic losses due to its impacts on animal welfare, ranging from poor meat quality to higher mortality rates (Geverink et al., 1998; Costa et al., 2016). The pre-slaughter stage is composed of a series of procedures in which the pigs are handled on the farm for loading, followed by transport and unloading at the slaughterhouse. These activities are uncommon and stressful events in the pigs' lives and must be well-planned and professionally carried out to avoid decreasing animal welfare (Ludtke et al., 2010; Costa et al., 2016; Ludtke et al., 2016).

Pigs are usually loaded and unloaded from trucks using ramps with a maximum inclination angle of 20º, preferably lower than 13º, with non-slip rubberized or embossed floors, and should be led in small groups, with the number of animals depending on the width of the corridor and the dock. This step should be carried out with the help of boards and compressed air prods to incentive movement and avoid abrupt stops. These guidelines are essential to minimize stress during loading and unloading (Correa et al., 2010; Ludtke et al., 2010; Ricci & Costa, 2015; Costa et al., 2016). However, handlers may still use electric prods to stimulate the movement of pigs and accelerate the loading process, which leads to increased heart rate, and negative changes in blood parameters, such as higher blood lactate and salivary cortisol concentrations, as well as carcass damage and inferior meat quality post-mortem, mainly when used by untrained handlers (Geverink et al., 1998; Correa et al., 2010; Ludtke et al., 2010; Costa et al., 2016; Goumon & Faucitano, 2017; European Commission, 2018). The use of modern vehicles with tailgate lifts for loading and unloading has been reported as a viable alternative to conventional ramps, with the benefit of reducing heart rate since the pigs do not need to climb or descend slopes (Garcia & McGlone, 2015). This system also contributes to easier handling and reduced loading/unloading times with minimum need for coercion by the staff (Gispert et al., 2000; Brown, Knowles, Wilkins, Chadd, & Warriss, 2005; Costa et al., 2016).

This work aimed to assess the preliminary mechanical aspects of using a scissor lift system for pre-slaughter pig handling due to its similarity to the tailgate lift mechanism and the possibility of use with conventional trucks. The term ‘scissor’ comes from the ability of the device to open (expand) and close (contract) as a scissor which is achieved by the use of linked, folding supports in a cross ‘X’ pattern (Arunkumar, Kartheeshwaran, & J, 2021; Pappalardo, La Regina, & Guida, 2023). This lift mechanism is capable of moving in the vertical plane by the application of force to one or more supports. The force used to expand the scissors mechanism may be hydraulic, pneumatic, or mechanical via a lead screw and pinion system (Dengiz, Şenel, Yıldızlı, & Koç, 2018; Ismael, Almaged, & Mahmood, 2019). A scissor lift system based on a standard design was used (Čuchor, Kučera, & Dzimko, 2021), and the design parameters were defined according to the desired application of loading and unloading pigs for transport. The mechanical analysis and the material selection process allowed the correct dimensioning and provided a structure capable of performing its function adequately and in a safe manner.

Material and methods

Design parameters and considerations

The scissor lift consists of a base platform, which supports the entire device, the scissors legs, and the top platform. This system must present a rigid and steady structure to maintain stability and reduce vibrations during operation since inadequate suspension can affect animal welfare by inducing nausea and muscular fatigue (European Commission, 2018). The platform's minimum width should be in the range of 1.0 to 1.1 m, considering a maximum width of 45-50 cm per pig, making it possible for at least two animals to pass simultaneously, which prevents the loss of visual contact with each other. The internal boarding dock walls must have approximately 1 m of height to avoid pigs jumping over during handling and relocation (Costa et al., 2016).

The walls on the same side as the scissor legs were set to be used as ramps to avoid gaps and to ease loading the pigs into the lift and unloading into the truck. These ramps were designed to result in an inclination angle lower than 15º and with grooves on the surface to prevent slipping. The system was designed considering an initial height of 0.25 m and working height of 1.2 m, with a platform length of 2.0 m and width of 1.6 m, to accommodate 3 pigs at a time and to fit traditional trucks, which feature mean deck width and height of 2.4 and 1.0 m, respectively (Costa et al., 2016). The proposed scissor lift design used in the analysis is illustrated in Figure 1.

In the case of loading pigs for transport, the maximum load capacity of the scissor lift is defined by the number of pigs in each group (n = 3) and their average weight (120 kg), along with the weight of the boarding dock platform and walls. The total load generated by the animals' weight was calculated using a safety factor of 1.5 to take into account the natural variability observed in large groups (Goumon & Faucitano, 2017). Therefore, the force generated by the weight of the pigs (W_P) was calculated using Equation 1, resulting in a force of $W_P = m \times g = (120 \times 3 \times 1.5) \times 9.81 = 5297.4\ N$. The force generated by the weight of the boarding dock materials was determined after the material selection process, which will be presented later.

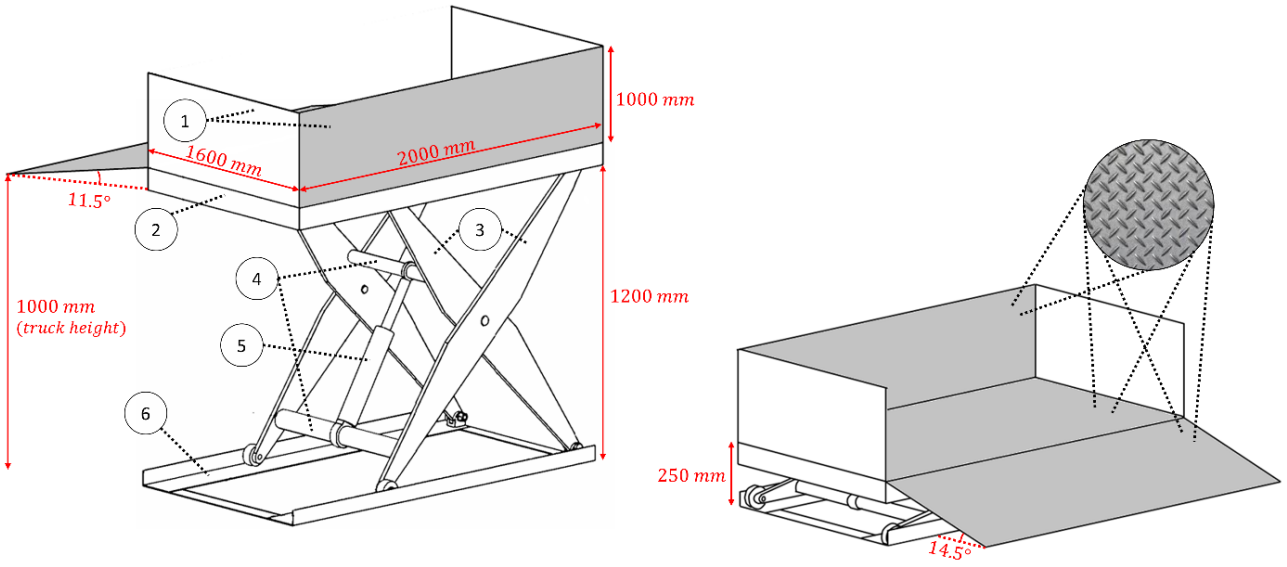

Figure 1. Scheme of the scissor lift design with its main components and dimensions: 1. Boarding dock walls, 2. Boarding dock platform, 3. Legs, 4. Supporting tubes, 5. Hydraulic Cylinder, 6. Base.

$$P = m \times g \quad (1)$$

where:
g is the acceleration of gravity, being adopted the value of 9.81 $\frac{m}{s^2}$ and m is the mass to be lifted.

Mechanical analysis

The situations of maximum load and bending moment of a scissor lift system are set to happen when the lift is stationary at its lowest and highest positions, respectively. Therefore, the scissor lift system was modeled as a rigid body, and the mechanical analyses were performed primarily considering the static forces in these two positions: the highest when the lift meets the truck's first floor; and the lowest when it is closed and lying on the floor. The reactions and internal forces, along with their evolution during the lift's movement, were also calculated. Figure 2 presents the free body diagram of the lift at its lowest position.

The wheels in points A and D allow the lift legs to open and close. The legs are connected by a pin at Point J and are fixed to the top and bottom platforms in points B and C, respectively. The member EF is the hydraulic cylinder and has a different angle to the leg angle. The support reactions analyses show that A and D are roller supports and B, C and J are pin supports. The total load weight (W_L) (total weight of pigs plus boarding dock) acts at the top platform's center of gravity and is transmitted to the legs structure. The load weight is divided by 2 since the lift system is symmetrical, and only one side is represented in Figure 2. For the lowest position, when the scissor is closed, the weight of the legs (structure weight) (W_S) acts in the same action line of W_L force. These two forces ($W_L + W_S$) are transmitted equally to A and B supports.

Static equilibrium of a body requires a balance of forces ($\vec{F}$) and moment ($\vec{M}$). The force balance prevents the body from translating or having accelerated motion along a straight or curved path. The balance of moments prevents the body from rotating. These conditions are expressed mathematically as the equations of equilibrium (Equation 2 and 3) (Hibbeler & Schiavone, 2004).

$$\sum \vec{F} = 0 \quad (2)$$

$$\sum \vec{M} = 0 \quad (3)$$

The Reaction forces in D and C were determined by considering the sum of moment and forces at point C, as expressed in Equation 4-11.

$$\sum M_c = 0 \quad (4)$$

$$-D_y . d + (W_L + W_S) . \frac{d}{2} = 0 \quad (5)$$

$$D_y = \frac{(W_L + W_S)}{2} \quad (6)$$

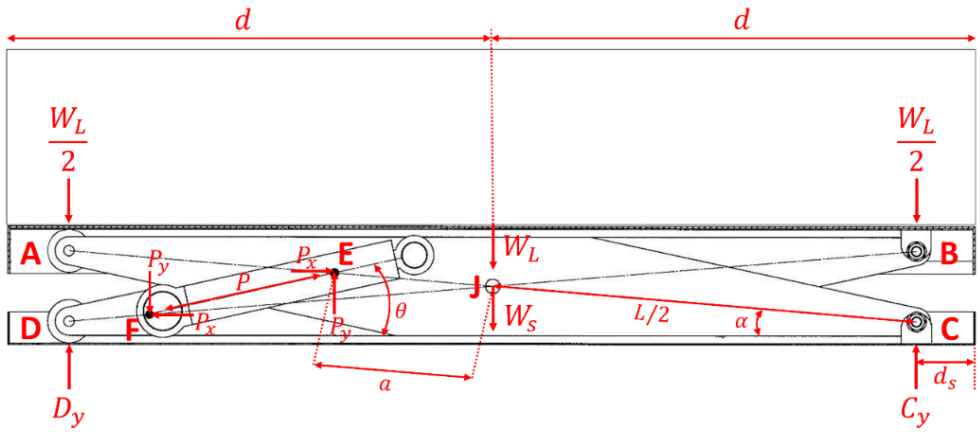

Figure 2. Free body diagram of the lift at the lowest position.

$$\sum F_y = 0 \tag{7}$$

$$D_y - (W_L + W_S) + C_y = 0 \tag{8}$$

$$\frac{(W_L+W_S)}{2} - (W_L + W_S) + C_y = 0 \tag{9}$$

$$C_y = \frac{(W_L+W_S)}{2} \tag{10}$$

$$D_y = C_y = \frac{(W_L+W_S)}{2} \tag{11}$$

The force (P) generated by the hydraulic cylinder activity acts directly on points E and F and contribute to the internal reaction forces acting at point J. The hydraulic cylinder is a two-force member (Hibbeler & Schiavone, 2004), and the force and moment equilibria are satisfied only if the two forces present the same magnitude and act in opposite directions. Hence, $P_E = P_F = P$ and share the same line of action along the line joining points E and F. These forces were decomposed into x and y components for the analysis, as described in Equation 12 and 13.

$$P_x = P\ cos\ \theta \tag{12}$$

$$P_y = P\ sin\ \theta \tag{13}$$

In the pin joint J, the internal reaction forces can be decomposed as J_x and J_y, which values and directions are not known yet. These forces are responsible to keep the legs together and to allow the opening and closing movements for the scissors. J_x and J_y can be calculated using the legs dimensions and projections (Equation 14 and 15) and the moment and force equilibria equations, as shown in Equation 14-23.

$$L_x = L\ cos\ \alpha \tag{14}$$

$$L_y = L\ sin\ \alpha \tag{15}$$

$$\sum F_x = 0 \tag{16}$$

$$P_x - J_x = 0 \tag{17}$$

$$J_x = P_x \tag{18}$$

$$J_x = P\ cos\ \theta \tag{19}$$

$$\sum F_y = 0 \tag{20}$$

$$-\frac{W_L}{2} + P_y - J_y - \frac{W_S}{2} + C_y = 0 \tag{21}$$

$$-\frac{(W_L+W_S)}{2} + P\ sin\ \theta\ - J_y + \frac{(W_L+W_S)}{2} = 0 \tag{22}$$

$$J_y = P\ sin\ \theta \tag{23}$$

The force P can be determined by considering the moment at point J and using the following geometry rule $(sin\ \theta\ .cos\ \alpha\ + cos\ \theta\ .sin\ \alpha\ ) = sin\ (\theta + \alpha)$, as shown in Equation 24-30.

$$\sum M_J = 0 \tag{24}$$

$$\frac{W_L}{2}.\left(\frac{L}{2}cos\ \alpha\ \right) - P_y.a\ cos\ \alpha\ + C_y.\left(\frac{L}{2}cos\ \alpha\ \right) - P_x.a\ sin\ \alpha\ = 0 \tag{25}$$

$$\frac{W_L}{4}L\ cos\ \alpha\ - P\ sin\ \theta\ .a\ cos\ \alpha\ + \frac{(W_L+W_S)}{2}.\left(\frac{L}{2}cos\ \alpha\ \right) - P\ cos\ \theta\ .a\ sin\ \alpha\ = 0 \tag{26}$$

$$\frac{W_L}{4}L\ cos\ \alpha\ + \frac{W_L}{4}L\ cos\ \alpha\ + \frac{W_S}{4}L\ cos\ \alpha\ - P.a(sin\ \theta\ .cos\ \alpha\ + cos\ \theta\ .sin\ \alpha\ ) = 0 \tag{27}$$

$$\frac{W_L}{2}L\ cos\ \alpha\ + \frac{W_S}{4}L\ cos\ \alpha\ - P.a\ sin\ (\theta + \alpha)\ = 0 \tag{28}$$

$$\left(\frac{W_L}{2} + \frac{W_S}{4}\right)L\ cos\ \alpha\ - P.a\ sin\ (\theta + \alpha)\ = 0 \tag{29}$$

$$P = \left(\frac{W_L}{2} + \frac{W_S}{4}\right)\frac{\alpha}{asin\ (\theta+\alpha)} \tag{30}$$

Figure 3 presents the free body diagram of the lift in the highest position, and Equation 31-51 present the determination of forces for this situation, similarly to what was done for the lowest position.

The Reaction forces in D and C can be determined by considering the moment at point C and the sum of forces in the y axis (Equation 31-37).

$$\sum M_c = 0 \tag{31}$$

$$-D_y.d_1 + W_L.d_2 + W_S.d_3 = 0 \tag{32}$$

$$D_y = \frac{(W_L.d_2+W_S.d_3)}{d_1}, with\ d_1 > d_2 > d_3 \tag{33}$$

$$\sum F_y = 0 \tag{34}$$

$$D_y - (W_L + W_S) + C_y = 0 \tag{35}$$

$$C_y = (W_L + W_S) - D_y \tag{36}$$

$$C_y = (W_L + W_S) - \frac{(W_L.d_2+W_S.d_3)}{d_1} \tag{37}$$

The internal reaction forces in point J can be determined by using the static equations of equilibrium in the x and y axis, as shown in Equation 38-45.

$$\sum F_x = 0 \tag{38}$$

$$P_x - J_x = 0 \tag{39}$$

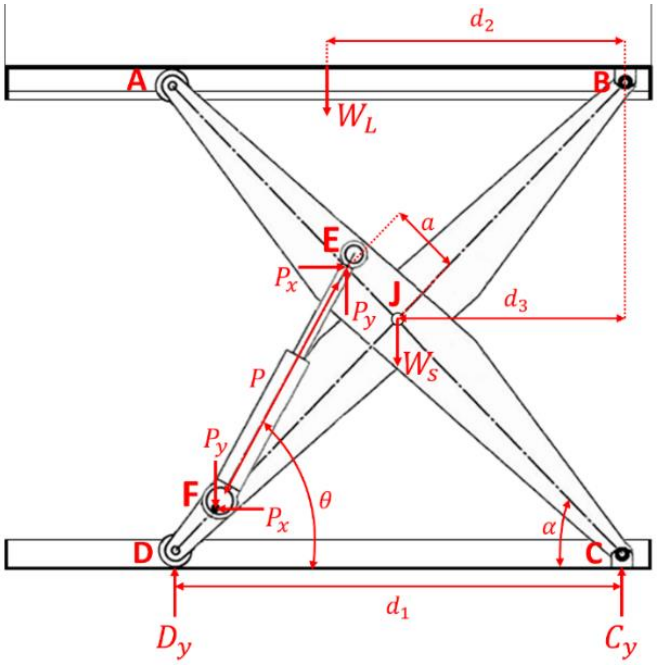

Figure 3. Free body diagram of the lift in the highest position.

$$J_x = P_x \quad (40)$$

$$J_x = P\ cos\ \theta \quad (41)$$

$$\sum F_y = 0 \quad (42)$$

$$-D_y + P_y - J_y - \frac{W_S}{2} + C_y = 0 \quad (43)$$

$$-\frac{(W_L.d_2+W_S.d_3)}{d_1} + P\ sin\ \theta\ - J_y - \frac{W_S}{2} + (W_L + W_S) - \frac{(W_L.d_2+W_S.d_3)}{d_1} = 0 \quad (44)$$

$$J_y = P\ sin\ \theta\ + W_L + \frac{W_S}{2} - 2 \cdot \frac{(W_L.d_2+W_S.d_3)}{d_1} \quad (45)$$

The force P can be determined by considering the moment at point J and using the following geometry rule ($sin\ \theta\ .cos\ \alpha\ + cos\ \theta\ .sin\ \alpha\ ) = sin\ (\theta + \alpha)$, as shown in Equation 46-51.

$$\sum M_J = 0 \quad (46)$$

$$D_y.\left(\frac{L}{2} cos\ \alpha\ \right) - P_y.a\ cos\ \alpha\ + C_y.\left(\frac{L}{2} cos\ \alpha\ \right) - P_x.a\ sin\ \alpha\ = 0 \quad (47)$$

$$\left(D_y+C_y\right)\frac{L}{2} cos\ \alpha\ - P\ sin\ \theta\ .a\ cos\ \alpha\ - P\ cos\ \theta\ .a\ sin\ \alpha\ = 0 \quad (48)$$

$$\left[D_y + (W_L + W_S) - D_y\right]\frac{L}{2} cos\ \alpha\ - P.a(sin\ \theta\ .cos\ \alpha\ + cos\ \theta\ .sin\ \alpha\ ) = 0 \quad (49)$$

$$(W_L + W_S)\frac{L}{2} cos\ \alpha\ - P.a\ sin\ (\theta + \alpha)\ = 0 \quad (50)$$

$$P = (W_L + W_S)\frac{Lcos\ \alpha}{2asin(\theta+\alpha)} \quad (51)$$

Materials selection

The objective of the materials selection analysis was to minimize the mass of the structural components of the lift while attending the mechanical constraints of the project. Steel and aluminum were initially selected due to their high strength and light weight, respectively, as well as their commercial availability in diverse shapes and sizes. Table 1 presents the typical properties for these materials (Ashby, 2011).

Table 1. Material properties (Ashby, 2011).

Material	$\rho\ (kg\ m^{-3})$	$E\ (GPa)$	$\sigma_y\ (MPa)$	v
Aluminum	2700	70	120	0.35
Steel	8750	200	320	0.30

In the case of the boarding dock, the floor and the walls are shaped as panels, which have specified length (L) and width (b), but no determined thickness (h). These panels are loaded in bending when supporting the pigs, so the stiffness constraint sets the maximum deflection (δ) allowed. Material index equations were used to assess the suitability of each material using the objective function presented in Equation 52 to minimize mass (Ashby, 2011).

$$m = AL\rho = bhL\rho \quad (52)$$

The constraints for stiffness (S) and strength (F) are presented in Equation 53 and 54, respectively, and the second moment of area (I) in Equation 55 (Ashby, 2011).

$$S = \frac{C_1 EI}{L^3} \quad (53)$$

$$F = 2C_2\frac{I\sigma_y}{bhL} \quad (54)$$

$$I = \frac{bh^3}{12} \quad (55)$$

where:
C_1 and C_2 are constants that depend on the distribution of the loads.

The mass of the panels can be reduced by reducing the thickness (h), but limited to the constraints. The performance equations can be obtained by combining Equation 52 with Equation 53 and 54, and eliminating the free variable h, as shown in Equation 55 and 56, in which the material index is in bold (Ashby, 2011).

$$m_1 = \left(\frac{12S}{C_1 b}\right)^{\frac{1}{3}} bL^2 \left(\frac{\rho}{E^{\frac{1}{3}}}\right) \quad (56)$$

$$m_2 = \left(\frac{6Fb}{C_2}\right)^{\frac{1}{2}} L^{\frac{3}{2}} \left(\frac{\rho}{\sigma_y^{\frac{1}{2}}}\right) \quad (57)$$

The cross-section of the lift legs (Figure 2) is rectangular and can be solid or hollow, however, the latter presents a higher shape-efficiency factor in bending ($\emptyset_B^e$), which leads to the development of lower bending stresses under the action of the same bending moment, by distributing the mass away from the center of gravity (Ashby, 2011). The bending factor of a solid and a hollow rectangular section is shown in Figure 4.

The parameters of the Rectangular Hollow Section (RHS) were determined by applying the slenderness limit for b/t (Zhao, Wilkinson, & Hancock, 2005), which is shown in Equation 58, to prevent buckling before the yield stress is reached, and by analyzing the real stresses in the structure calculated from the mechanical analysis.

$$\frac{b}{t} \leq \sqrt{\frac{k\pi^2 E}{12(1-v^2)\sigma_y}} \quad (58)$$

where:
k is a constant dependent on stress distribution, E is the elastic modulus, v the Poisson ratio, and σ_y is the yield stress.

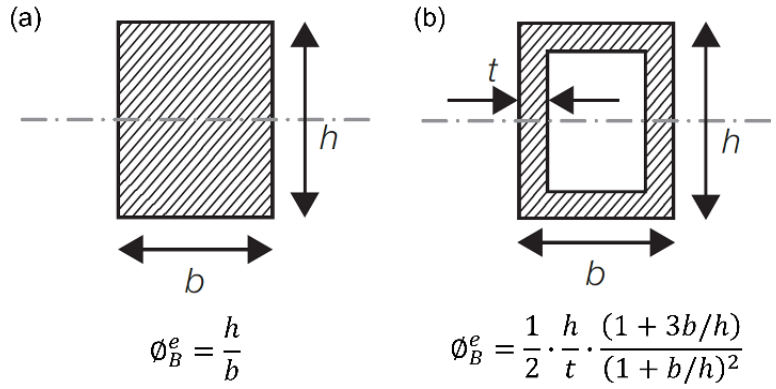

Figure 4. Shape-efficiency factors in bending ($\emptyset_B^e$) for (a) solid and (b) hollow rectangular sections (Ashby, 2011).

Selection of size for pins, bearings, and hydraulic piston rod

The size of the pins used to fix the legs at points B and C, the size of the central pin located in point J, as well as the size of the pins used to fix the wheels at points A and D were estimated based on the condition of use (single or double shear) along with the calculated loads and the allowable stresses for each material.

The hydraulic cylinder acts as a bar with pinned ends and is subjected to direct compressive force which may lead to buckling in the rod. Euler's method of calculation was used to estimate the size of the hydraulic cylinder's buckling load (Equation 59) (Hibbeler, 2016).

$$F_k = \frac{\pi^2 \times E \times I}{sf \times L_k^2} \quad (59)$$

where:
F_k is the admissible buckling load, E the elastic modulus, I the moment of inertia of rod, sf the safety factor, and L_k the free buckling length.

The free buckling length is a function of the measured length of the rod, L, and the effective length factor, K. The effective length factor is obtained using the boundary conditions applied to the hydraulic cylinder, i.e., the fixations of cylinder and piston rod have to be considered. In this case, $K = 1$ since the hydraulic cylinder is pinned ends (Hibbeler, 2016). The moment of inertia of a rod with circle cross-section is given by Equation 60 and the piston rod diameter d can be estimated by Equation 61.

$$I = \frac{\pi \times d^4}{64} \quad (60)$$

$$d = \left(\frac{64 \times F_k \times L_k^2 \times sf}{\pi^3 \times E}\right)^{\frac{1}{4}} \quad (61)$$

Results and discussion

The results from the materials selection process for the boarding dock platform and larger lateral walls, which are highlighted in Figure 1 with darker shades, are presented in Table 2. Equation 55 and 56 were used along with the properties presented in Table 1 and the following variables: $L = 1.6\ m$, $b = 2.0\ m$, $C_1 = 384/5$, $C_2 = 24$, $F = W_P = 5297.4\ N$, $S = 1.589.10^6\ N/m$.

Table 2. Results of the performance equations for reducing mass.

Material	$m_1\ (kg)$	$t_1\ (mm)$	$m_2\ (kg)$	$t_2\ (mm)$
Aluminum	167.3	19.37	16.34	2.97
Steel	342.9	13.65	29.09	1.82

The minimum possible weight for the panels to meet both constraints, for a given material, is determined by the larger of m_1 or m_2. In this case, stiffness is the limiting constraint, and aluminum yields the lighter components. The minimum thickness of these panels was set as 20 mm ($m_p = 2\ m \times 1.6\ m \times 0.02\ m \times 2700\ kg/m^3 = 172.8\ kg, m_{lw} = 2 \times [2\ m \times 1\ m \times 0.02\ m \times 2700\ kg/m^3] = 216\ kg$). Pinus wood ($\rho = 420\ kg\ m^{-3}, t = 20\ mm$) was selected as the material for the smaller boarding dock walls to reduce weight, since these components are not structural ($m_{sw} = 2 \times [1.6\ m \times 1\ m \times 0.02\ m\ \times 420\ kg/m^3] = 26.88\ kg$). The total load ($W_L$) to be lifted is comprised of the pigs' weight (W_P) and the weight of the entire boarding dock, aluminum platform and walls and Pinus wood walls: $W_L = W_P + g(m_p + m_{lw} + m_{sw}) = 5297.4 + 9.81(172.8 + 216 + 26.9) = 9375.4\ N$.

After determining W_L, the weight of the legs structure (W_S) was defined based on the legs' geometry and section shape. The slenderness limit (Equation 58) for the RHS was calculated using the materials properties from Table 1 and $k = 0.425$ (Zhao et al., 2005), and yielded the following guideline: $t \geq 0.065\ b$. Figure 5 presents the bending factor calculated for a solid and a hollow section varying the width (b) in function of the height (h) (Figure 4), and using the slenderness limit for the hollow section.

The maximum bending factor for the solid section is 4 when $b = 0.25h$, which is 8 times lower than the value for the hollow section ($\emptyset_B^e = 32$). Therefore, the RHS was selected and the mass of the legs structure was calculated based on $b = 0.25h$ and $t = 0.07b$. The calculated mass of one leg was 17.97 and 6.18 kg for steel and aluminum, respectively. The weight of the legs structure for each material was: $W_{S\ steel} = 9.81(4 \times 17.97) = 705\ N$ and $W_{S\ Al} = 9.81(4 \times 6.18) = 242\ N$. A structure made of aluminum yields a lower weight, but the predominant force acting on the system originates from the boarding dock load (W_L). This way, the difference between $W_{S\ steel}$ and $W_{S\ Al}$ is not significant to the real loads acting on the structure and the strength constraint becomes more important, indicating that steel may be the best choice, as it will be discussed later (Table 4 and Figure 9 and 10).

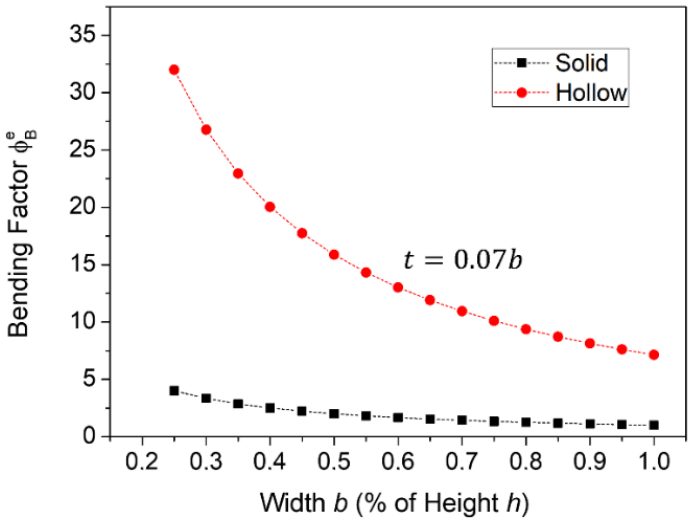

Figure 5. Shape-efficiency factor in bending ($\emptyset_B^e$) for a solid and a hollow section.

The force (P) generated by the hydraulic cylinder activity was calculated based on W_L and W_S (Equation 30 and 51), its (θ) and the legs angle (α), the leg length ($L = 1.7\ m$), and the distance (a) between point E and J (Figure 2 and 3). Table 3 presents the values of each variable used in the calculation of P during the movement of the lift from the lowest to the highest position, and Figure 6 shows its evolution in function of the legs angle (α), both considering legs made of steel. The situation of maximum load happens when the lift is at its lowest position. The selected maximum height of the lift (1.2 m) (Figure 1) leads to the following values: $\theta = 53°$, $\alpha = 43°$, $a = 0.125$ m, and $P = 48.6\ kN$.

All the other forces acting on the structure were also calculated and are presented in Table 4. In the highest position, the distances indicated in Figure 3 are: $d_1 = 1243$, $d_2 = 850$, and $d_3 = 621$ mm.

All calculated forces must be decomposed into x' and y' components concerning the leg axis angle, using the rules of geometry, in order to determine the normal force, shear force, and bending moment diagrams, as well as the real stresses in the legs. Figure 7 shows the details of the force decomposition and the diagrams for one leg, while Figure 8 shows the same for the other leg. All the values presented in these Figures concern legs structures made of steel in the lowest position, which represents the maximum load condition. Negative and positive values indicate compressive and tensile forces, respectively.

Table 3. Values of the variables used in the calculation of force P.

Hydraulic cylinder angle (θ) (°)	Legs angle(α) (°)	Distance E-Ja(m)
13	5	0.309
19.4	10	0.222
25.6	15	0.191
31.4	20	0.172
36.5	25	0.160
41.5	30	0.149
46.2	35	0.135
50.3	40	0.126
54.6	45	0,115

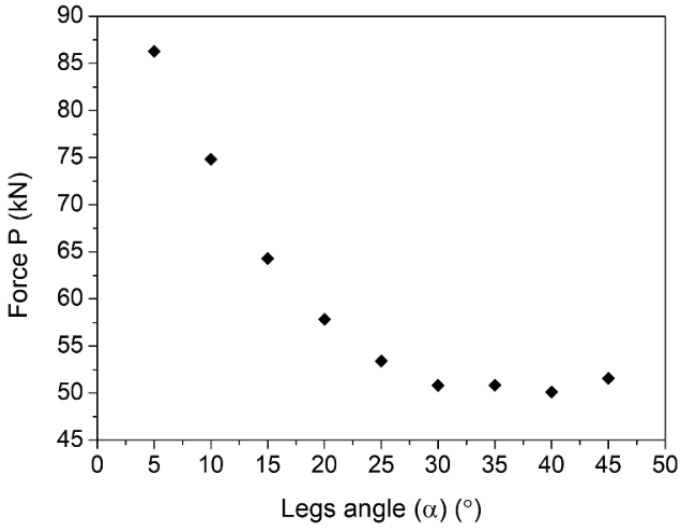

Figure 6. Evolution of the hydraulic cylinder force (P) during operation.

Table 4. Values of the forces acting on the lift at the lowest and highest positions.

Force (kN)	Aluminum structure		Steel structure	
	Closed (lowest)	Open (highest)	Closed (lowest)	Open (highest)
P	84.2	48.1	86.3	50.4
J_x	82.1	28.9	84.1	30.3
J_y	18.9	34.9	19.4	36.5
C_y	4.8	3.1	5.0	3.3
D_y		6.5		6.8

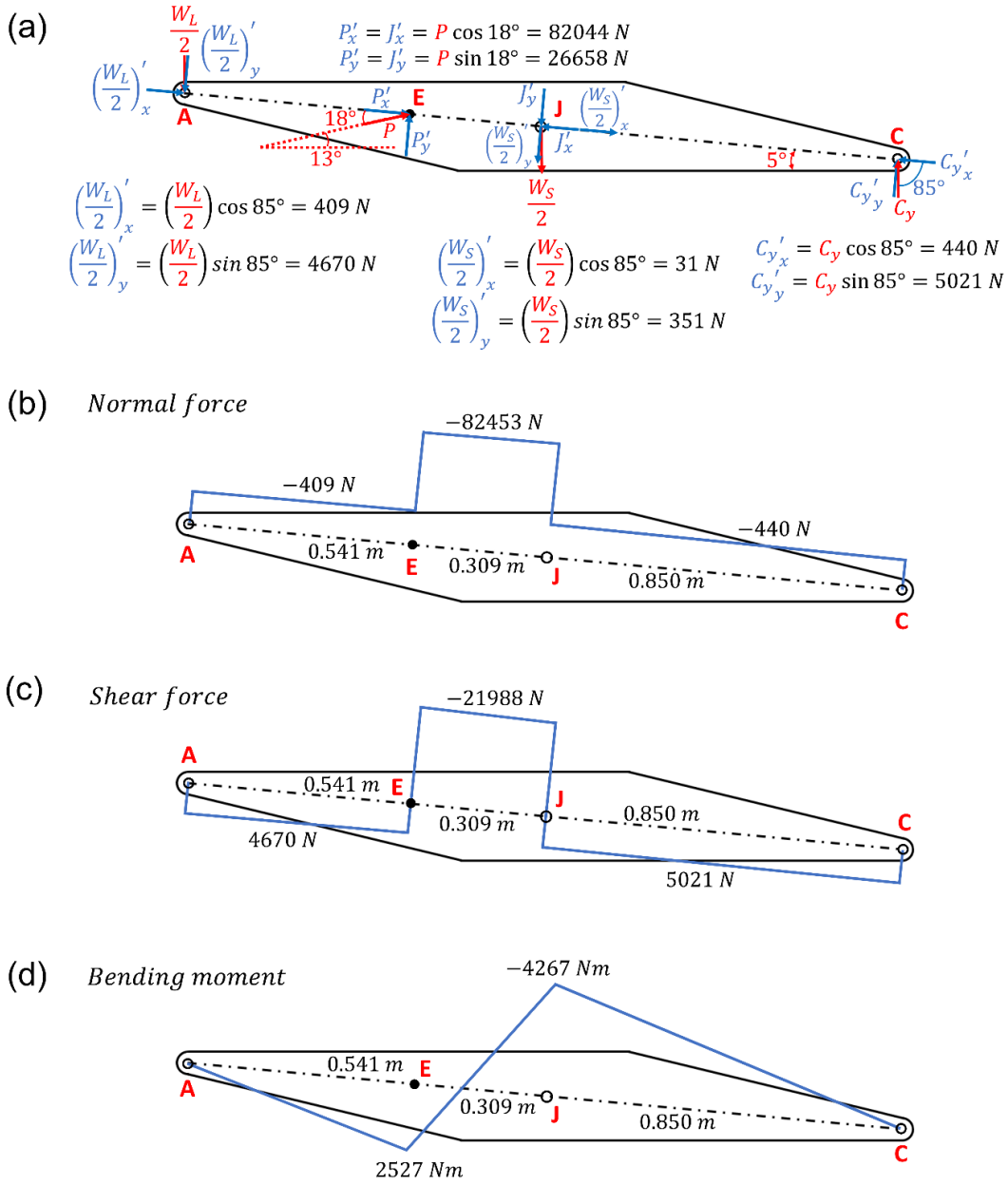

Figure 7. Scheme of the decomposition of forces to the components of the axis of the first leg in the lowest position (a), and the diagrams for (b) normal force, (c) shear force, and (d) bending moment.

The sections of the legs that are subjected to the highest forces are located between the points EJ and FJ, however, the cross-section areas in points E and F are the smallest, resulting in higher stresses. Figure 9 and 10 show the areas of these points and the stresses calculations for legs structures made of aluminum and of steel for comparison. The area is multiplied by 2 in the stresses calculations due to the fact that there are two symmetric legs in each side supporting the boarding dock. Table 5 presents the allowable normal stress with a safety factor of 3 and the shear stress calculated from the normal stress by applying a safety factor of 1.7.

Figure 11 presents schemes of the different loads acting on the pins at points A, B, C, D, and J, and on the hydraulic piston rod, along with the conditions of use. The pins in points B, C, and J are under double shear and the situation of maximum load (C_y and J, respectively) occurs when the lift is in the closed position (Figure 2). The pins in points A and D are under single shear and the maximum load (D_y) happens when the lift is open (Figure 3). The maximum load (P) acting on the piston is generated when the lift is closed (Table 4) and its minimum diameter was estimated based on the buckling load and the piston work length.

The minimum diameter of each pin was calculated using the loads presented in Table 4, which were divided by 2 to account for the symmetry of the system and each pair of points, and the allowable shear stresses of each material (Table 5). Regarding pins in points A and D, the shear stress is the limiting factor considering

that the radial stresses generated by a pin acting as a shaft for a plain bearing will be lower for any diameter larger than the minimum one calculated. The calculations presented in Figure 11 can be adjusted for any chosen material to guide for any other selection processes.

In general, structures made of steel are subjected to stresses well within the safety factors. The same happens to the aluminum legs, but with a lower margin of clearance, with the highest equivalent stress of 39.5 MPa nearing the allowable normal stress of 40 MPa. Besides, aluminum presents no endurance limit and tends to fail in fatigue after repeated cycles, even with small stress amplitudes, as opposed to steel. The only advantage of aluminum over steel in this case would be its natural resistance to rust and corrosion, since the weight difference does not impact significantly the forces acting on the lift structure. However, there are several successful strategies that can be adopted to avoid the issues of corrosion in steel structures, such as selecting adequate compositions of stainless steel as well as applying protective coatings.

The time for loading pigs in a truck using the proposed scissor lift can be estimated based on an average lifting time of 30 s for a maximum height of 1.2 m and faster descent with no pigs, considering that the average speed of 0.5 m s^{-1} for commercial pistons and the need of a slow ascent to account for the animals' welfare. Therefore, a group of 120 pigs could be loaded into a truck within 30 minutes, considering groups of 3 and an average time of operation of 40 seconds per group, which is similar to the time range when hydraulic systems are used (Costa et al., 2016) and slightly lower for when sloped ramps are used (Garcia & McGlone, 2015).

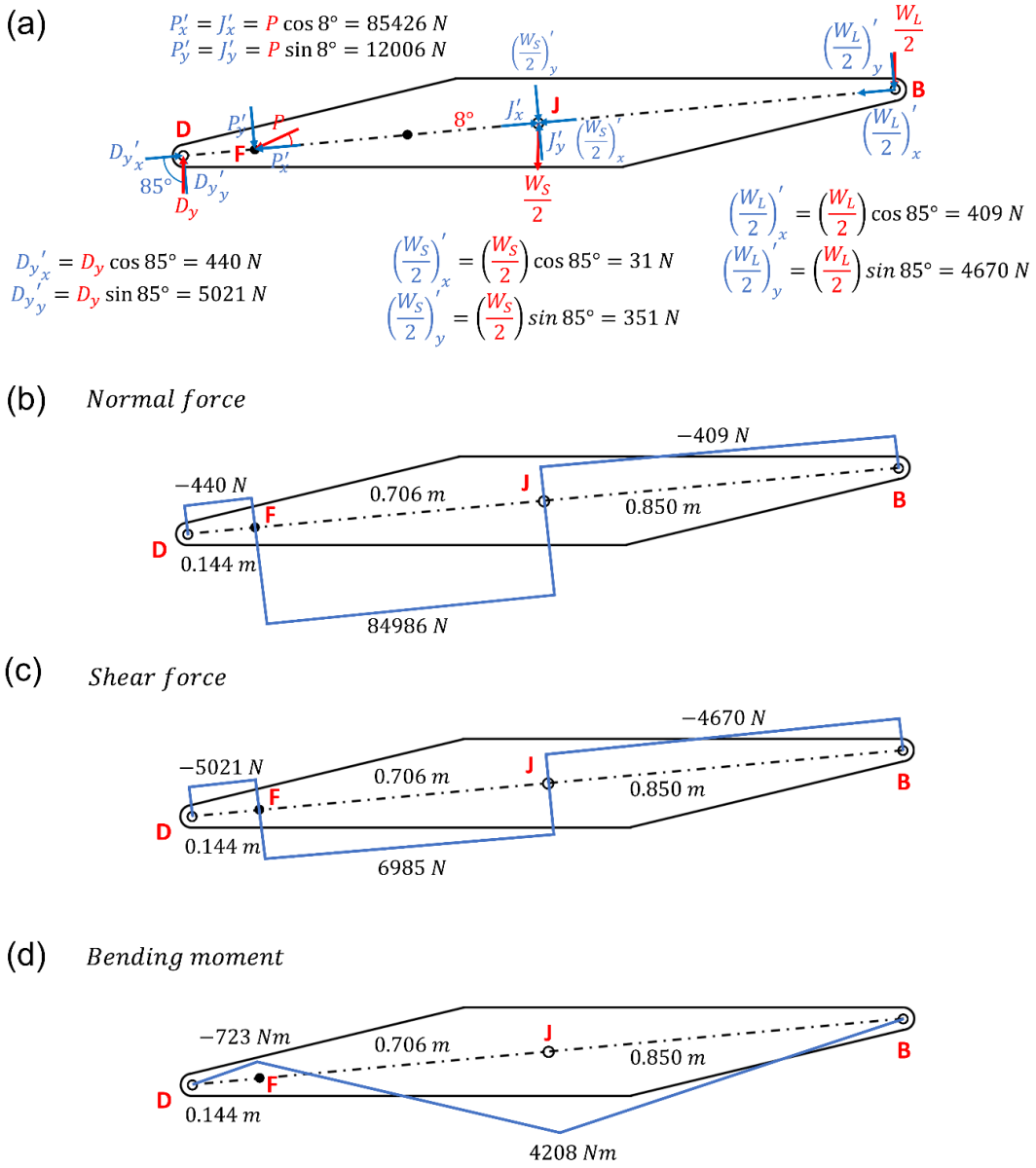

Figure 8. Scheme of the decomposition of forces to the components of the axis of the second leg in the lowest position (a), and the diagrams for (b) normal force, (c) shear force, and (d) bending moment.

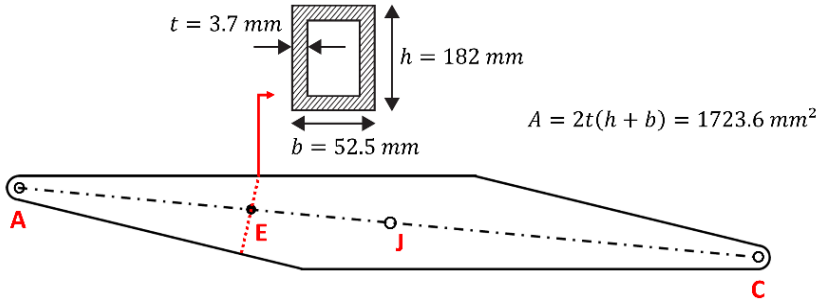

- ***Stresses in Point E***

- ***Aluminum***

$$\sigma_n = \frac{F}{2 \times A} = \frac{-80503\ N}{2 \times 1723.6\ mm^2} = -23.4\ MPa$$

$$\tau = \frac{F}{2 \times A} = \frac{-21354\ N}{2 \times 1723.6\ mm^2} = -6.2\ MPa$$

$$\sigma_{eq} = \sqrt{\sigma_n^2 + 3\tau^2} = 25.7\ MPa$$

- ***Steel***

$$\sigma_n = \frac{F}{2 \times A} = \frac{-82453\ N}{2 \times 1723.6\ mm^2} = -23.9\ MPa$$

$$\tau = \frac{F}{2 \times A} = \frac{-21988\ N}{2 \times 1723.6\ mm^2} = -6.4\ MPa$$

$$\sigma_{eq} = \sqrt{\sigma_n^2 + 3\tau^2} = 26.3\ MPa$$

$$\sigma_M = \frac{My}{2 \times I} \quad I = \frac{1}{6}h^3 t\left(1 + 3\frac{b}{h}\right)$$

$$\sigma_M = \frac{2527 \times 1000 \times 91}{2 \times \left[\frac{1}{6} \times 182^3 \times 3.7 \times \left(1 + 3 \times \frac{52.5}{182}\right)\right]} = 16.7\ MPa$$

Figure 9. Details of the cross-section area in Point E and the stresses calculations.

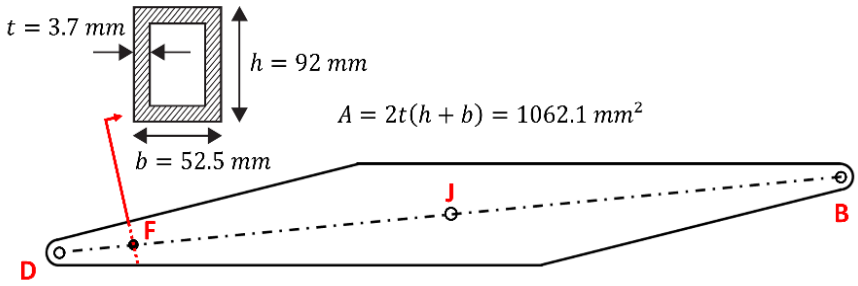

- ***Stresses in Point F***

- ***Aluminum***

$$\sigma_n = \frac{F}{2 \times A} = \frac{82977\ N}{2 \times 1062.1\ mm^2} = 39.1\ MPa$$

$$\tau = \frac{F}{2 \times A} = \frac{6930\ N}{2 \times 1723.6\ mm^2} = -3.3\ MPa$$

$$\sigma_{eq} = \sqrt{\sigma_n^2 + 3\tau^2} = 39.5\ MPa$$

- ***Steel***

$$\sigma_n = \frac{F}{2 \times A} = \frac{84986\ N}{2 \times 1062.1 mm^2} = 40.0\ MPa$$

$$\tau = \frac{F}{2 \times A} = \frac{6985\ N}{2 \times 1062.1 mm^2} = 3.3\ MPa$$

$$\sigma_{eq} = \sqrt{\sigma_n^2 + 3\tau^2} = 40.4\ MPa$$

$$\sigma_M = \frac{My}{2 \times I} \quad I = \frac{1}{6}h^3 t\left(1 + 3\frac{b}{h}\right)$$

$$\sigma_M = -12.3\ MPa \qquad \sigma_M = -12.9\ MPa$$

Figure 10. Details of the cross-section area in Point F and the stresses calculations.

Table 5. Allowable stresses for the materials.

Material	$\sigma_N = \frac{\sigma_y}{3}\ (MPa)$	$\tau = \frac{\sigma_N}{1.7}\ (MPa)$
Aluminum	40	24
Steel	107	63

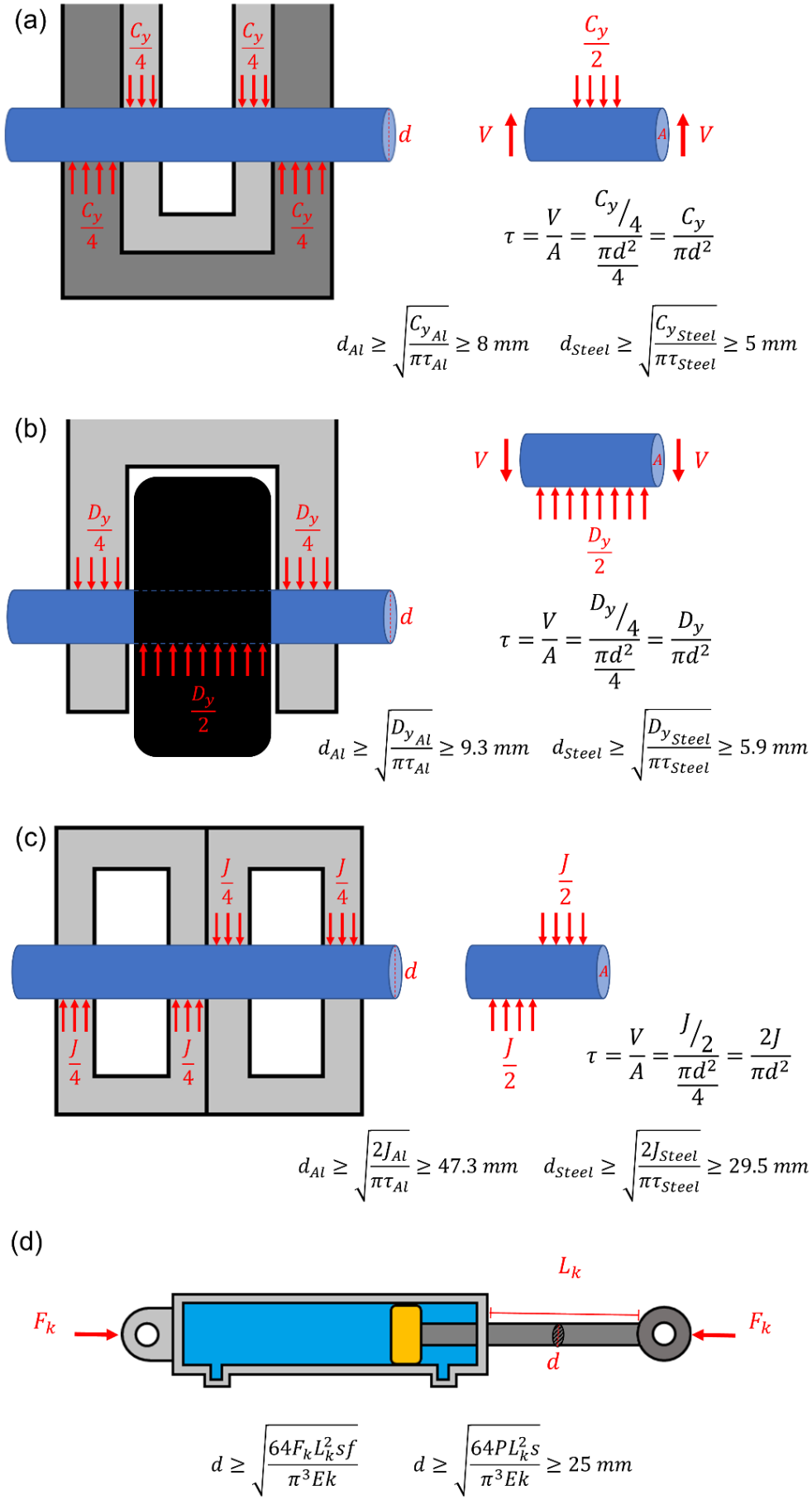

Figure 11. Scheme and calculations of minimum diameter of pins in points B and C (a), of pins in points A and D (b), of the central pin in point J (c), and for the piston rod (d).

Conclusion

The static analysis of the scissor lift mechanism for loading pigs for transport was carried out with analytics methods and provided the framework for this work. The materials selection process and the mechanical analysis allowed to determine the optimal sizing and design of the structural elements. These simple analyses, using analog calculations, lead to the development of a preliminary design for a practical scissor lift that represents an evolution from the sloped ramp method that is currently used, and allows a faster, more efficient, and safer way of loading and unloading, both for the pigs and for the handlers.

References

Arunkumar, G., Kartheeshwaran, R., & J, S. (2021). Investigation on design, analysis and topological optimization of hydraulic scissor lift. *Journal of Physics: Conference Series, 2054*(1), 012081. DOI: https://doi.org/10.1088/1742-6596/2054/1/012081

Ashby, M. F. (2011). *Materials selection in mechanical design* (4th ed.). Oxford, UK: Elsevier.

Brown, S. N., Knowles, T. G., Wilkins, L. J., Chadd, S. A., & Warriss, P. D. (2005). The response of pigs to being loaded or unloaded onto commercial animal transporters using three systems. *The Veterinary Journal, 170*(1), 91-100. DOI: https://doi.org/10.1016/j.tvjl.2004.05.003

Correa, J. A., Torrey, S., Devillers, N., Laforest, J. P., Gonyou, H. W., & Faucitano, L. (2010). Effects of different moving devices at loading on stress response and meat quality in pigs. *Journal of Animal Science, 88*(12), 4086-4093. DOI: https://doi.org/10.2527/jas.2010-2833

Čuchor, M., Kučera, Ľ., & Dzimko, M. (2021). Engineering design of lifting device weighing up to 3.5 tons. *Transportation Research Procedia, 55*, 621-628. DOI: https://doi.org/10.1016/j.trpro.2021.07.095

Costa, F. A. D., Costa, M. J. R. P., Faucitano, L., Costa, O. A. D., Lopes, L. S., & Renuncio, E. (2016). Ease of handling, physiological response, skin lesions and meat quality in pigs transported in two truck types. *Archivos de Medicina Veterinaria, 48*(3), 299-304. DOI: https://doi.org/10.4067/s0301-732x2016000300009

Costa, O. A. D., Costa, F. A. D., Holdefer, A. C., Jacob, J. S., Paweukievicz, L., & Buss, L. P. (2016). *Comunicado Técnico 532: embarcadouro para suínos em sistema de terminação*. Concórdia, SC: Embrapa.

Barcellos, M. D., Saab, M. S. M., Pérez-Cueto, F., Perin, M. G., Neves, M. F., & Verbeke, W. (2011). Pork consumption in Brazil: challenges and opportunities for the Brazilian pork production chain. *Journal on Chain and Network Science, 11*(2), 99-113. DOI: https://doi.org/10.3920/JCNS2011.Qpork3

European Commission. (2018). *Guide to good practices for the transport of pigs*. Publications Office. Retrieved from https://encurtador.com.br/mFLT1

Garcia, A., & McGlone, J. J. (2015). Loading and unloading finishing pigs: effects of bedding types, ramp angle, and bedding moisture. *Animals, 5*(1), 13-26. DOI: https://doi.org/10.3390/ani5010013

Geverink, N. A., Kappers, A., van de Burgwal, J. A., Lambooij, E., Blokhuis, H. J., & Wiegant, V. M. (1998). Effects of regular moving and handling on the behavioral and physiological responses of pigs to preslaughter treatment and consequences for subsequent meat quality. *Journal of Animal Science, 76*(8), 2080-2085. DOI: https://doi.org/10.2527/1998.7682080x

Gispert, M., Faucitano, L., Oliver, M. A., Guàrdia, M. D., Coll, C., Siggens, K., ... Diestre, A. (2000). A survey of pre-slaughter conditions, halothane gene frequency, and carcass and meat quality in five Spanish pig commercial abattoirs. *Meat Science, 55*(1), 97-106. DOI: https://doi.org/10.1016/s0309-1740(99)00130-8

Dengiz, C. G., Şenel, M. C., Yıldızlı, K., & Koç, E. (2018). Design and analysis of scissor lifting system by using finite elements method. *Universal Journal of Materials Science, 6*(2), 58-63. DOI: https://doi.org/10.13189/ujms.2018.060202

Goumon, S., & Faucitano, L. (2017). Influence of loading handling and facilities on the subsequent response to pre-slaughter stress in pigs. *Livestock Science, 200*, 6-13. DOI: https://doi.org/10.1016/j.livsci.2017.03.021

Zhao, X.-L., Wilkinson, T., & Hancock, G. (2005). *Cold-formed tubular members and connections: structural behaviour and design*. Oxford, UK: Elsevier Science.

Hibbeler, R. C. (2016). *Mechanics of materials* (10th ed.). New Jersey, US: Pearson.

Hibbeler, R. C., & Schiavone, P. (2004). *Statics study pack: chapter reviews, free body diagram workbook, problems website*. New Jersey, US: Pearson/Prentice Hall.

Ismael, O. Y., Almaged, M., & Mahmood, A. (2019). Quantitative design analysis of an electric scissor lift. *American Scientific Research Journal for Engineering, Technology, and Sciences, 59*(1), 128-141.

Ludtke, C. B., Ciocca, J. R. P., Dandin, T., Barbalho, P. C., Vilela, J. A., & Costa, O. A. D. (2010). *Abate humanitário de suínos*. Rio de Janeiro: WSPA.

Ludtke, C., Costa, O. A. D., Rohr, S. A., & Costa, F. A. D. (2016). *Bem-estar animal na produção de suínos: manejo de embarque e transporte para o frigorífico*. Brasília, DF: ABCS.

Ministério da Agricultura e Pecuária [Mapa]. (2021). *Projeções do agronegócio 2020-2021 a 2030-2031*. Recuperado de https://www.gov.br/agricultura/pt-br/assuntos/politica-agricola/todas-publicacoes-de-politica-agricola/projecoes-do-agronegociot

Pappalardo, C. M., La Regina, R., & Guida, D. (2023). Multibody modeling and nonlinear control of a pantograph scissor lift mechanism. *Journal of Applied and Computational Mechanics, 9*(1), 129-167. DOI: https://doi.org/10.22055/jacm.2022.40537.3605

Ricci, G. D., & Costa, O. A. D. (2015). Abate humanitário de suínos. *Revista de Ciências Agroveterinárias, 14*(3), 239-244.

Zanella, J. R. C. (2017). Pork production chain: importance and challenges faced. In *12th International Symposium on the Epidemiology and Control of Biological, Chemical and Physical Hazards in Pigs and Pork* (p. 21-25). Foz do Iguaçu.